Dalton Transactions

Accepted Manuscript

ROYAL SOCIETY OF CHEMISTRY

www.rsc.org/dalton

Journal Name

RSCPublishing

ARTICLE

Multi-component assembly and luminescence tuning of lanthanide hybrids based with both Zeolite L/A and SBA-15 through two organically grafted linkers

Cite this: DOI: 10.1039/xoxxoooooox

Received ooth January 2014,
Accepted ooth January 2014

DOI: 10.1039/xoxxoooooox

www.rsc.org/

Lei Chen, Bing Yan*

Both Zeolite A/L and SBA-15 have been used to assemble novel photofunctional multi-component lanthanide hybrid materials. Microporous zeolites A/L are firstly functionalized by embedding lanthanide or zinc complexes (TTA = thenoyltrifluoroacetone, TAA = trifluoroacetone, bipy = 2,2'-bipyridyl) into the pores of zeolite A/L and then the surface of functionalized zeolite A/L are modified via covalent linkers from aromatic carboxylic acids (para-aminobenzoic acid ABA and para-hydroxyl benzoic acid HBA) grafted by 3-(triethoxysilyl)-propyl isocyanate (TEPIC). On the other hand, SBA-15 is modified by grafting covalent linker phen-Si from the modification of 1,10-phenanthroline (phen) with TEPIC. Then another lanthanide ion is used to be linked both functionalized zeolites A/L and SBA-15 through the coordination with the two covalent linkers, ABS-Si (HBA-Si) and phen-Si, respectively. Subsequently, the obtained multicomponent microporous-mesoporous hybrid materials are assembled and characterized by means of XRD, FT-IR, UV-vis DRS, SEM, TEM and luminescent approaches (spectra, lifetimes and quantum efficiencies). These hybrids with both microporous zeolite and SBA-15 mesoporous host possess favourable luminescent performance and some hybrid systems present the high quantum efficiencies of 90 %. Besides, the luminescent color can be tuned by adjusting the composition of these hybrids, among which four hybrids (S-phen-Eu-HBA-[ZA-Tb-bipy] S-phen-Eu-HBA-[ZA-Zn-bipy], S-phen-Eu-ABA-[ZA-Tb-TAA], S-phen-Eu-ABA-[ZL-Tb-bipy]) can be integrated to white light emission.

Introduction

Lanthanide complexes have aroused great interest of many researchers because of their sharp and intense emission bands, a broad range of lifetime and high color purity.[1,2] Although organolanthanide complexes exhibit much more efficient emission under ultraviolet excitation, they have not been used directly in practical applications because of their poor thermal stability and low mechanical strength. In order to improve the thermal and luminescent stability of lanthanide complexes, lanthanide inorganic–organic hybrid materials are developed, which can integrate the respective characteristics of inorganic and organic parts and result in their outstanding properties. So they have many potential applications in the fields such as in optical amplifiers, light-conversion molecular devices and light-conversion molecular devices *etc*.[3-6] For these hybrids, the key is to design a functional linker that can coordinate and sensitize lanthanide ions, assembling the whole hybrid system.[7-9]

To obtain such requirements, much research work on lanthanide inorganic–organic hybrid materials incorporation has been done in the past decades.[3-12] Mesoporous silica such as MCM-41, SBA-15, POMs and microporous zeolites can behave as the host for organolanthanide lanthanide complexes, whose host-guest hybrid materials present interesting luminescence properties and embody them great potential for practical application.[13-15] The hybrid materials enable both inorganic and organic dopants to be incorporated with relatively high thermal stability. Zeolites are crystalline microporous materials with highly regular nanometer-sized channels or cavities inside, which are widely used in a variety of applications for their unique porous properties.[16] Assembly of organolanthanide complexes into different types of zeolite microcrystals has attracted much attention in recent years because they can be further modified to be applied as hosts for supramolecular organization of guest molecules or nanostructures, among which zeolite L (ZL) crystals have played a great role in the construction of luminescent materials due to their special structures.[17] ZL crystals feature perfect one-dimensional and strictly parallel channels arranged in hexagonal symmetry and has proven to be an ideal host of hybrid materials with intriguing properties.[18] ZL is easily to be functionalized with targeting groups for its surface is covered with a large number of hydroxyls and luminescent lanthanide complexes can be inserted into the one-dimensional channels via the ''ship in a bottle method''.[19] However, little attention has been paid to the assembly of lanthanide complexes into the zeolite A (ZA) crystals.[20] ZA, an aluminosilicate with unique pore size and high capacity of ion exchange, has of a great potential

in the encapsulation and assembly of lanthanide complexes.[21] It's necessary to study this system and to shed some light on its optical properties.

On the other hand, some mesoporous molecular sieves possess ordered arrays of uniform nanochannels and can be used as a support for organolanthanide lanthanide complexes.[22] Among all of the mesoporous materials, SBA-15 pays much more attractive than other mesoporous silica because of its adjustable pore size (3 to 30 nm), large pore-size mesochannel, thick silica wall and high thermal stability.[23] Both mesoporous silica SBA-15 and microporous zeolite have a large number of hydroxyls, which can be easily further functionalized to assemble hybrid materials. Based on zeolite and SBA-15's ability of self-assembly of commonality, they can be linked together by silica coupling agent and coordination of lanthanide ion. The new synthetic micro-mesoporous hybrid materials have the advantages over either microporous or mesoporous materials.

Herein, we prepare a series of lanthanide micro-mesoporous hybrid materials, which are named as S-phen–Ln-L2-[ZA/L-Ln/Zn-L1] (S = SBA-15, Ln = Eu/Tb, L1 = TTA (thenoyltrifluoroacetone) / TAA (trifluoroacetone) / bipy (2,2'-bipyridyl), L2 = HBA (*para* hydroxyl benzoic acid) / ABA (*para* aminobenzoic acid)) through the multi-component assembly strategy. The motivation behind the idea is to study micro-mesoporous hybrid materials as the host of lanthanide complexes and the photophysical properties of the hybrid systems. The physical characterization and luminescent properties are discussed and compared in details.

Experimental section

Starting materials Chemical pure and highly crystalline zeolite L crystals were synthesized according to a previously reported procedure.[24] Disc-shaped and nanosized crystals (500 nm) were used in this study. $LnCl_3{\cdot}6H_2O$ (Ln = Eu and Tb) were obtained by dissolving their respective oxides (Eu_2O_3 and Tb_4O_7) in concentrated hydrochloric acid. 3-(Triethoxysilyl)-propyl isocyanate (95 %, TEPIC), 1,10-phenanthroline monohydrate (99 %, phen), thenoyltrifluoroacetone (99 %, TTA) and 1,1,1-trifluoroacetylacetone (98 %, TAA) were from Adamas. Sodium hydroxide, potassium hydroxide and sodium metaaluminate were from Aladdin. Colloidal silica (40 %, Ludox HS-40) was from Sigma and Pluronic P123 was from Lancaster Synthesis Ltd). Other reagents were analytically pure and purchased from China National Medicines Group.

Synthesis of the molecular linkage phen-Si The precursor phen-Si was prepared according to the previous literature.[7a] The ^{1}H NMR ($CDCl_3$, 400 MHz) data of phen-Si were as follows: 0.54 (4H, m), 1.15 (18H, t), 1.60 (4H, m), 3.24 (4H, m), 3.73 (12H, q), 7.24 (2H, s), 7.68 (2H, m), 7.89 (1H, s), 8.26 (2H, m), 9.25 (2H, m).

Synthesis of the phen-functionalized SBA-15 mesoporous material (phen-SBA-15) The SBA-15 mesoporous material was prepared with the following molar composition:[15c] 0.0172 P123: 0.96 TEOS: 0.04phen-Si: 6HCl: 208.33H_2O. 1.0 g P123 was firstly dissolved in deionized water (7.5 g) and 2 mol·L^{-1} HCl solution (30 mL) at 308 K. Then a mixture of TEOS and phen-Si was added into the above solution drop by drop at 308 K with stirring for 24 hrs. After that the mixture was transferred into a Teflon bottle sealed in an autoclave for the hydrothermal reaction for 48 hrs at 373 K. The solid product was washed with deionized water thoroughly after filtration, and air-dried at 333 K for 12 hrs. Removal of copolymer surfactant P123 was conducted by Soxhlet extraction with ethanol for 48 hrs. The obtained material phen-SBA-15 was dried at 353 K in a vacuum.

Synthesis of the hybrid materials ZA/L-Ln-L1 The ZL-Ln^{3+} and ZA-Ln^{3+} samples were prepared by ion-exchange.[19,20] 100 mg of zeolite L or zeolite A was stirred in an aqueous solution of $LnCl_3{\cdot}6H_2O$ (20 mL of a 0.10 M) for 12 hrs at 353 K. The product was collected by centrifugation, then washed with deionized water by three times and dried at 353 K under atmospheric conditions. The samples were firstly degassed and dried for 2 hrs at 423 K to get rid of the solvent molecules in zeolite channels, and then it was exposed to the TTA (phen) vapor at 453 K for 18 hrs, or exposed to TAA vapor at 353 K for 18 hrs. The hybrid material was washed with dichloromethane till the filtrate became colorless, and then dried at 313 K under vacuum for 4 hrs.

Synthesis of the molecular linkage HBA-Si and ABA-Si HBA-Si was synthesized by the modification of HBA by TEPIC.[25] 2.0 mmol para-hydroxybenzoic acid (0.279 g) was first dissolved in 20 mL acetone by stirring and then 2.0 mmol of TEPIC (0.497 g) was added to the solution dropwise. The whole mixture was continued to reflux in a covered flask under argon atmosphere at 333 K for approximately 13 hrs. Finally, the objective product was obtained after centrifugation and purification. Yield 68 %. The ^{1}H NMR ($CDCl_3$, 400 MHz) data of HBA-Si are as follows: d 0.63 (2H, t), 1.29 (9H, t), 1.65 (2H, m), 2.93 (2H,t), 3.74 (6H, m), 3.98 (1H, t), 6.82 (2H, d), 7.79 (2H, d), 10.24 (1H, s). The modified ABA (ABA-Si) was prepared as follows: [27] 1 mmol ABA (0.139 g) was first dissolved in 20 mL $CHCl_3$ with stirring. Then, 2.0 mmol (0.497 g) of TEPIC was added into the refluxing solution dropwise. The mixture was heated at 350 K in a covered flask under nitrogen atmosphere for 12 hrs. After isolation and purification, ABA-Si was obtained. The ^{1}H NMR ($CDCl_3$, 400 MHz) data of ABA-Si are as follows: d 0.69 (4H, t), 1.11 (18H, t), 1.43 (4H, m), 3.20 (4H,t), 3.84 (12H, m), 4.12 (2H, t), 7.46 (2H, d), 8.02 (2H, d).

Synthesis of the hybrid materials HBA-[ZA/L-Ln-L1] and ABA-[ZA/L-Ln-L1] (L1 = phen/TTA/TAA). HBA-Si (0.6 g) and ZA/L-Ln-L1 (3.4 g) were dissolved in 4 mL acetone by stirring at 383 K for approximately 4 hrs. The objective product was obtained after centrifugation and purification, and then dried at 383 K for 12 hrs obtained the final material.

Preparations of S-phen–Ln1-L2-[ZA/L-Ln2(Zn)-L1] (Ln = Eu/Tb/Zn; L1 = bipy/TTA/TAA; L2 = HBA/ABA). The modified zeolite (0.6 g) and phen-SBA15 were dissolved in 20 mL THF by stirring, and then 2.0 mL 0.1 M of $LnCl_3$ (Ln = Eu or Tb)was added to the solution dropwise, continuously stirring at 333 K for about 12 hrs. The product was obtained after centrifugation and purification obtained the final material. The contents of Ln^{3+} ions (Ln = Eu, Tb) in the hybrids are determined as following with the coordination titration and the content of N element can be determined. It is hardly to determine the exact composition of them within the complicated hybrid system, but the content of Ln^{3+} and N are the content unlike C or H elements, which cannot change with the difference of the sol-

gel process. So the molar ratio of Ln and N can be used to predict the ratio of Ln^{3+} and S-phen unit and HBA-Si (or ABA-Si) unit in the mesoporous hybrid system, proving the key coordination environment surrounding of lanthanide ions between S-phen and HBA-Si (or ABA-Si). For S-phen-Tb-HBA-[ZA-Eu-TTA]: Tb 3.31 %, N 1.99 %; for S-phen-Tb-ABA-[ZL-Zn-bipy]: Tb 3.65 %, N 4.40 %; for S-phen-Eu-HBA-[ZA-Tb-bipy]: Eu 3.40 %, N 3.03 %; for S-phen-Eu-HBA-[ZA-Zn-bipy]: Eu 3.51 %, N 3.45 %; for S-phen-Eu-ABA-[ZA-Tb-bipy]: Eu 3.41 %, N 3.80 %; for S-phen-Eu-ABA-[ZL-Tb-bipy]: Eu 3.32 %, N 3.77 %; for S-phen-Eu-ABA-[ZA-Tb-TAA]: Eu 3.36 %, N 3.04 %. According to the content of Ln^{3+} and N, it can be predicted the molar ratios of Ln: N for S-phen-Tb-HBA-[ZA-Eu-TTA] and S-phen-Eu-ABA-[ZA-Tb-TAA] are close to 1: 7 and 1:10, while for the hybrids with bipy, the molar ratios of Ln: N are close to 1: 11 for HBA-Si linker and 1: 14 for ABA-Si. According to the molar ratio values, it can be predicted that the nitrogen atoms comes from S-phen (four N atoms), HBA-Si (three N atoms) or ABA-Si (six atoms) and about two bipy ligands to provide four N atoms. Therefore, it can demonstrate that the coordination environment surrounding scheme of the composition of the mesoporous hybrid system.

Physical characterization The Fourier transform infrared spectra (FTIR) were measured within KBr slices from 4000 to 400 cm^{-1} region using a Nexus 912 AO446 infrared spectrum radiometer. ^1H NMR spectra were recorded in $CDCl_3$ on a BRUKER ARX400 spectrometer with tetramethylsilane (TMS) as inter reference. The elemental analyses of nitrogen element the hybrids are measured with a CARIO-ERBA 1106 elemental analyser. The contents of Ln^{3+} ions (Eu^{3+}, Tb^{3+}) in the hybrids were determined with ICP-OES and the molar ratio in the hybrids could be estimated. Luminescence (excitation and emission) spectra and luminescence lifetime measurements were carried out on an Edinburgh FLS920 phosphorimeter using a Xenon lamp as the excitation source, whose powers are 450 W and 100 mW, respectively. The outer luminescent quantum efficiency was determined using an integrating sphere (150 mm diameter, $BaSO_4$ coating) from Edinburgh FLS920 phosphorimeter. The spectra were corrected for variations in the output of the excitation source and for variations in the detector response. The quantum yield can be defined as the integrated intensity of the luminescence signal divided by the integrated intensity of the absorption signal. The absorption intensity was calculated by subtracting the integrated intensity of the light source with the sample in the integrating sphere from the integrated intensity of the light source with a blank sample in the integrating sphere. X-ray powder diffraction patterns (XRD) were recorded on Rigaku D/max-Rb diffractometer equipped with Cu anode, and the data were collected within the 2θ range of 0.6 – 6.0 °. The ultraviolet–visible diffuse reflective absorption spectroscopy (UV–vis DRS) were acquired on B&WTEKO BWS003 UV-vis diffuse reflectance spectroscopy from 800 to 200 cm^{-1}. Scanning electronic microscope (SEM) images were obtained by a Hitachi S-4800. Transmission electron microscope (TEM) experiments are performed using a JEOL2011 microscope operated at 200 kV.

Results and discussion

The schematic representation of selected multi-component hybrid material S-phen-Ln-ABA-[ZA-Zn/Ln-L] is shown in Figure 1. Here it is an example and other hybrids are similar except for the change of different lanthanide ions or zeolite (ZL) or different ligands. (Figure S1 shows the typical scheme for detailed synthesis process of the organically modified silane linkers phen-Si, HBA-Si, ABA-Si, functionalized microporous zeolite L/Z and mesoporous SBA-15 (HBA-[ZA/L-Ln-L1] (a), ABA-[ZA/L-Ln-L1] (b) and phen-SBA-15 (c) and final hybrids S-phen–Ln-HBA-[ZA/L-Ln-L1] (d) and S-phen–Ln-ABA-[ZA/L-Ln-L1] (e)) For such a multicomponent hybrid system with complicated composition, it is difficult to confirm their exact structures. However, according to lanthanide coordination chemistry principle and functional units, it is possible to determine the main composition and the basic chemical linking mode between different building units in these hybrids. Initially, Eu-TTA, Tb-TAA, Tb-bipy or Zn-bipy complexes are loaded into the channels of zeolite A or zeolite L host, forming ZA/L-Zn/Ln-L1 (L1 = bipy, TTA, TAA) hybrids. Afterwards, the external surfaces of ZA-Ln-L1 or ZL-Ln-L1 are modified with functional covalent linkers HBA-Si or ABA-Si through the reaction between triethoxysilyl group of TEPIC unit and the hydroxy groups from zeolite surface. On the other hand, SBA-15 is modified by phen-Si linker through the cohydrolysis and copolycondensation reaction between their both alkoxy groups. Finally, the multi-component hybrids are assembled by the connection of modified zeolite and SBA-15 via the coordination between the lanthanide ions and HBA(ABA) groups grafted in ZA/L as well and phen groups of phen-SBA-15. Here each lanthanide ions are coordinated to six oxygen atoms from three functionalized linkers HBA-Si (or ABA-Si) and two nitrogen atoms from one from phen-Si linker. The chelation effect between Ln^{3+}, HBA-Si(ABA-Si) and phen-Si is easily formed and the molar ratio 1: 3: 1 of Ln^{3+}: HBA-Si(ABA-Si): phen-Si can occupy eight coordination position of Ln^{3+}, similar with typical lanthanide complexes of small molecule ligands of HBA(ABA) and phen. [26] This can be evidenced by the elemental data of Ln^{3+} and N atoms for these hybrid systems. (See above experimental section)

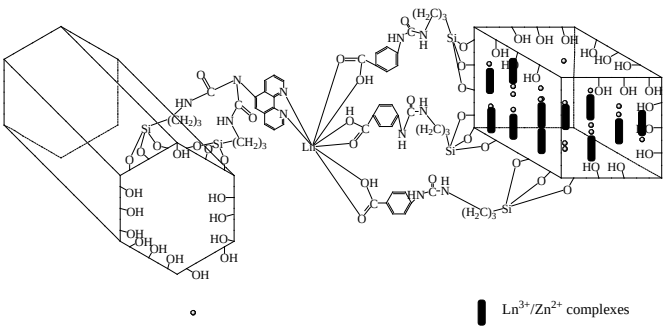

Figure 1 Schematic representation of the selected micro-mesoporous hybrid materials S-phen-Ln-ABA-[ZA-Ln/Zn-L].

Figure S2 (a) shows the FT-IR spectra of the free ligand phen-NH_2 (A) and the precursor phen-SBA-15 (B). The presence of the organic ligand phen covalently bonded to the mesoporous SBA-15 was characterized by IR absorption spectra. In view of free ligand phen-NH_2, the absorption bands at 3416 and 3324 cm^{-1} corresponds to the stretching vibration of the NH_2 group of phen-NH_2. It can be observed that the vibrations of NH_2 were replaced by a wide peak at

3446 cm^{-1} in phen-SBA-15, which indicates the formation of hydroxyl groups (-OH).[7c,27] For phen-SBA-15 material, a series of absorption bands at 2983, 2949 and 2879 cm^{-1} are due to the symmetric of the methylene (-CH_2-) groups. In addition, new peaks at 1079 (ν_{as}, Si-O), 801 (ν_s, Si-O) and 463 cm^{-1} (ν, Si-O-Si) are due to the formation of the Si-O-Si framework. Furthermore, the peaks at 1636 and 1558 cm^{-1} originating from the -CONH- group can also be observed in hybrid mesoporous material phen-SBA-15, which is consistent with the fact that phen group in the framework remains intact after both hydrolysis-condensation reaction and the surfactant extraction procedure.[7c,27] The FT-IR spectra of seven kinds of hybrid materials are presented in Figure 2. The similar infrared spectra appear because of their similar framework. The evident bands appearing at 1082 and 796 cm^{-1} are attributed to the asymmetric Si-O stretching vibration modes and the symmetric Si-O stretching vibration, respectively. The bands centered at 463 cm^{-1} correspond to the bending vibration of Si-O-Si, and the bands at 963 cm^{-1} are due to silanol (Si-OH) stretching vibrations of surface groups. The water molecules present in the samples are evidenced by the stretching and the bending vibrations at about 3445 and 1642 cm^{-1}, respectively. Compared with phen-SBA-15, the hybrid materials not only exhibit the similar infrared absorption bands as the silica framework but also enhance relative intensities of bands, which indicate that europium (III) complexes have been grafted onto the wall of SBA-15 and zeolite.

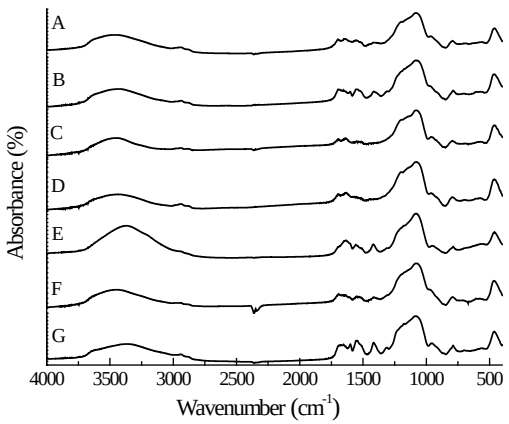

Figure 2 The IR spectra of microporous-mesoporous hybrid materials S-phen-Tb-HBA-[ZA-Eu-TTA] (A), S-phen-Tb-ABA-[ZL-Zn-bipy] (B), S-phen-Eu-HBA-[ZA-Tb-bipy] (C), S-phen-Eu-HBA-[ZA-Zn-bipy] (D), S-phen-Eu-ABA-[ZA-Tb-bipy] (E), S-phen-Eu-ABA-[ZL-Tb-bipy] (F), S-phen-Eu-ABA-[ZA-Tb-TAA] (G).

Figure 3 shows the selected SAXRD patterns of hybrid materials S-phen-Eu-HBA-[ZA-Tb-bipy], S-phen-Eu-ABA-[ZL-Tb-bipy] and S-phen-Tb-ABA-[ZL-Zn-bipy]. All these hybrid materials exhibit the similar diffraction peaks in the 2θ range of 0.6–2 °, which are characteristic of SBA-15-type two-dimensional hexagonal (P6mm), index as the (100), (110), and (200) diffractions. The d_{100} spacing values of the hybrid materials prove that the framework hexagonal ordering has been kept well[28] upon the introduction of organolanthanide complexes and modified ZL or ZA. New hybrid materials still have a high physical and chemical stability of mesoporous microstructure.

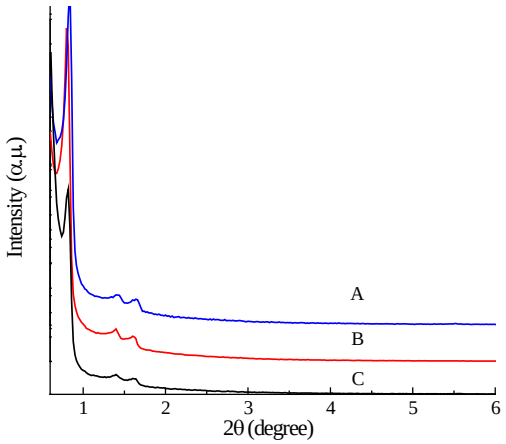

Figure 3 The selected SAXRD patterns of S-phen-Tb-ABA-[ZL-Zn-bipy] (A), S- phen-Eu-HBA-[ZA-Tb-bipy] (B), S-phen-Eu-ABA-[ZL-Tb-bipy] (C).

SEM images of ZL, ZA and the selected hybrid materials (S-phen-Eu-ABA-[ZL-Tb-bipy], S-phen-Eu-HBA-[ZA-Tb-bipy]) are shown in Figure S3 (a), (b), (c) and (d), respectively. An SEM image of the ZL used in this study is given in Figure S3 (a), which illustrates the disc-shaped form of the crystals with a length between 200 and 500 nm and a diameter in the order of 300 nm. An SEM image of ZA is shown in Figure S3 (b), in which we can see the shape morphology of ZA is the typical truncated cubes with an average dimension of 2000 nm. The SEM of the selected two hybrid materials reveal aggregates composed of zeolite and SBA-15 in Figure S3 (c) and (d). The hybrid materials no longer keep the complete regular crystal shape of zeolite. The hexagonal porous structure of S-phen-Eu-HBA-[ZA-Tb-bipy] is further confirmed by its selected TEM micrograph (see Figure 4), which is also agreement with the result of SAXRD. As shown in the figure, S-phen-Eu-HBA-[ZA-Tb-bipy] presents a regular hexagonal array of uniform channels characteristic of mesoporous SBA-15 material. The distance between the centers of the mesopore is estimated to be 10 nm, in good agreement with the value determined from the corresponding SAXRD data. These photos illustrate that the mesostructure of the micro-mesoporous complex materials can be substantially conserved after the coordination process.

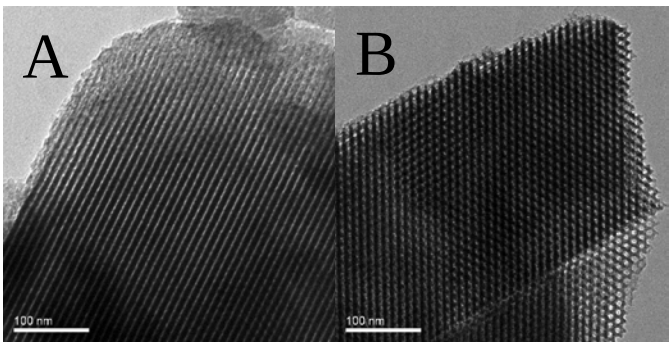

Figure 4 The selected TEM images of S-phen-Eu-HBA-[ZA-bipy-Tb] along the [100] (A) and [110] (B) zone axes.

Figure S4 (a) presents the selected ultraviolet-visible diffuse reflective absorption spectra (UV-vis DRS) of hybrids with Zn^{2+} complexes loaded zeolite, S-phen-Eu-HBA-[ZA-Zn-bipy] (A) and S-phen-Tb-ABA-[ZL-Zn-bipy] (B). Both of them show a large broad

absorption band from 250 to 500 nm which partially overlap with the excitation spectra (wide band at 250 to 500 nm in following excitation spectra). It also has a little sharp emission band at 617 nm for S-phen-Eu-HBA-[ZA-Zn-bipy], which overlaps with the emission line of Eu^{3+}. The S-phen-Eu-HBA-[ZA-Zn-bipy] shows a large broad absorption band from 250 to 350 nm and a sharp emission band at 544 nm. The hybrid materials could absorb abundant energy in ultraviolet–visible extent and transfer the energy to the corresponding rare earth ions by the so-called ‘‘antenna effect”. Figure S4 (b) shows the selected ultraviolet-visible diffuse reflective absorption spectroscopy of the hybrids with Ln^{3+} loaded zeolite. These hybrid materials exhibit a large broad absorption band from 250 to 550 nm and a sharp emission band at 613 nm which overlap with their luminescence spectra.

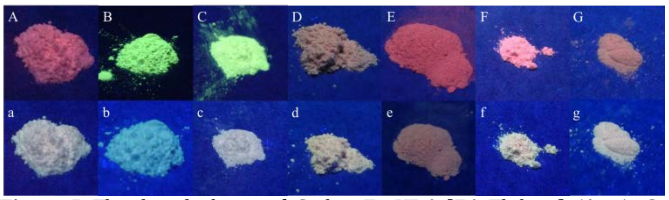

Figure 5 The digital photos of S-phen-Eu-HBA-[ZA-Tb-bipy] (A, a), S-phen-Tb-ABA-[ZL-Zn-bipy] (B, b), S-phen-Tb-HBA-[ZA-Eu-TTA] (C, c), S-phen-Eu-ABA-[ZL-Tb-bipy] (D, d), S-phen-Eu-ABA-[ZA-Tb-bipy] (E, e), S-phen-Eu-HBA-[ZA-Zn-bipy] (F, f), S-phen-Eu-ABA-[ZA-Tb-TAA] (G, g) under UV irradiation (λ_{ex} = 254, 365nm).

Seven kinds of materials display strong and bright emission color upon irradiation by a UV lamp (254, 365 nm), as shown in Figure 5. Powder product was putted on the weighing paper, and then it was under the UV lamp directly to take pictures. Different materials have different light color in the same conditions for the imparity of host material, lanthanide ion and organic ligand modified linkers. The same material under the different wavelengths of exciting light also displays two kinds of emitting light. Photographs of the photoluminescent color from the materials imply that the procedure used in this study can offer a facile way to control the exciting light of luminescent materials through a choice of the reaction precursor and exciting light. But for the limited and fixed excitation spectra, whose matching degree with the excitation spectra of these hybrids may affect the photographs of their emission color. The exact study will be seen from the CIE diagram from the emission spectra of these hybrids.

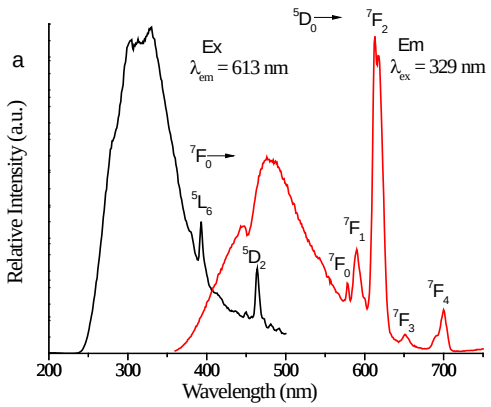

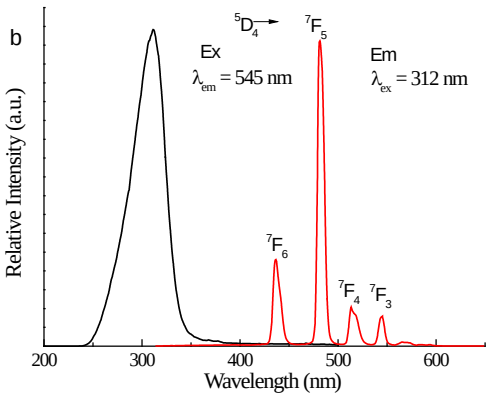

Figure 6 Luminescent spectra of hybrid materials S-phen-Eu-HBA-[ZA-Zn-bipy] (a) and S-phen-Tb-ABA-[ZL-Zn-bipy] (b).

Figure 6 shows the excitation and emission spectra of the two hybrids with Zn^{2+} complex loaded zeolites, S-phen-Eu-HBA-[ZA-Zn-bipy] (a) and S-phen-Tb-ABA-[ZL-Zn-bipy] (b). The excitation spectrum of S-phen-Eu-HBA-[ZA-Zn-bipy] is obtained by monitoring the $^5D_0 \rightarrow {}^7F_2$ transition line at 613 nm, and the emission spectrum was obtained by excitation at 329 nm. A broad band ranging from 230 to 500 nm is mainly from the HBA unit to form charge transfer state of Eu-O, whose wide excitation is favourable for the energy transfer and luminescence of Eu^{3+} in the hybrid system. Furthermore, two weak sharp excitation lines overlapped with the wide band at 393 nm and 464 nm can be observed, which correspond to f-f ($^7F_0 \rightarrow {}^5L_6$ and $^7F_0 \rightarrow {}^5D_2$) transitions of Eu^{3+} ion, respectively.[29] The corresponding emission spectrum consists of a broad band ranging from 370 to 570 nm and five prominent lines at 578, 590, 613, 651 and 700 nm. The former wide band emission is originated from the organically modified hosts of phen-SBA-15 and HBA-[ZL-Zn-bipy], whose two emission peaks suggests the two origins from different host factors. The latter can be ascribed to the $^5D_0 \rightarrow {}^7F_0$, $^5D_0 \rightarrow {}^7F_1$, $^5D_0 \rightarrow {}^7F_2$, $^5D_0 \rightarrow {}^7F_3$ and $^5D_0 \rightarrow {}^7F_4$ transitions of Eu^{3+}. The hypersensitive forced electronic dipole $^5D_0 \rightarrow {}^7F_2$ transition shows the highest emission intensity. It is worthy pointing out the existence of the wide emission from host can provide the possibility to integrate with the red emission of Eu^{3+} to tune emission color or even display white luminescence. The luminescence data of the S-phen-Tb-ABA-[ZL-Zn-bipy] are shown in Figure 6 (b). Different from Figure 6 (a), its excitation spectra obtained by monitoring the $^5D_4 \rightarrow {}^7F_5$ at 545 nm show the narrow band ranging from 250 to 350 nm, which is ascribed to the $\pi \rightarrow \pi$ electron transition of organic ligands phen and ABA units. No detectable absorption lines of Tb^{3+} ions can be observed from the excitation spectra, indicating that an effective energy transfer occurs from phen or ABA unit to Tb^{3+} ions. Under the excitation using this broad band of 312 nm, four sharp emission lines at 489, 544, 583 and 622 nm appear, which can be ascribed to the transitions of Tb^{3+}: $^5D_4 \rightarrow {}^7F_6$, $^5D_4 \rightarrow {}^7F_5$, $^5D_4 \rightarrow {}^7F_4$ and $^5D_4 \rightarrow {}^7F_3$, respectively. The emission intensity for $^5D_4 \rightarrow {}^7F_5$ transition shows the highest, which can account for the characteristic green color of Tb^{3+} observed upon the ultraviolet irradiation of 254 nm as seen in Figure 5.

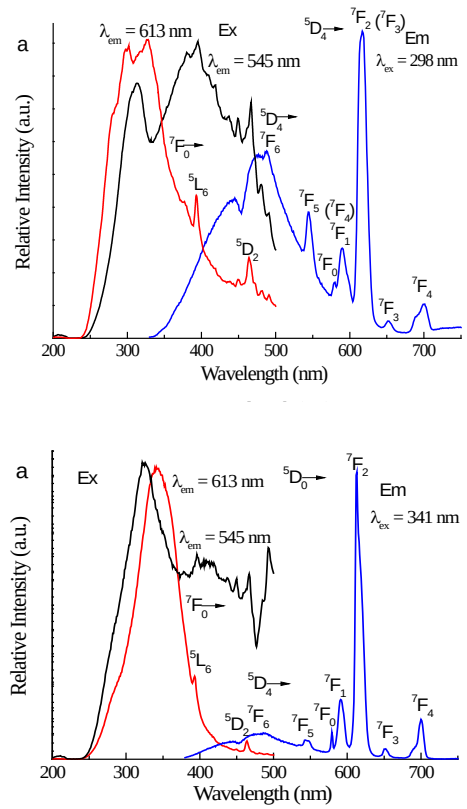

Figure 7 Luminescent spectra of hybrid material (a) S-phen-Eu-HBA-[ZA-Tb-bipy] and (b) S-phen-Eu-ABA-[ZA-Tb-bipy].

Figure 7 (a) shows the excitation and emission spectra of S-phen-Eu-HBA-[ZA-Tb-bipy] hybrids. The two kinds of excitation spectra are obtained by selectively monitoring the $^5D_0 \rightarrow {}^7F_2$ transition line at 613 nm of Eu^{3+} and the $^5D_4 \rightarrow {}^7F_5$ transition line at 545 nm of Tb^{3+}, respectively. For the excitation spectrum for Eu^{3+}, it shows the similar feature to that in Figure 6(a), a wide broad excitation covering 230 ~ 500 nm for the HBA (CTS of Eu-O) and phen unit, together with excitation lines at 393 nm and 464 nm of Eu^{3+} ions can be observed from the excitation spectra, which can be ascribed to ineffective energy transfer occurs from phen to the f-f ($^7F_0 \rightarrow {}^5L_6$ and $^7F_0 \rightarrow {}^5D_2$) transitions of Eu^{3+} ions.[29] For the excitation spectrum for Tb^{3+}, a complicated excitation spectrum is obtained. The excitation band at 310 nm may be originated from organic ligands (bipy). Besides, the apparent broad excitation band extends to visible region, which may be related to the organically modified host (HBA-ZL and S-phen). Considering both excitation spectra, we select 298 nm as λ_{ex} to measure the emission spectrum for it is suitable for both Eu^{3+} and Tb^{3+}. The emission is similar with that of Figure 6 (a). The wide band is ascribed as total emission of the organically modified hosts of phen-SBA-15 and HBA-ZL, and two emission peaks stands for the two origins from different host factors. Moreover, the characteristic emissions of Tb^{3+} (489 nm, $^5D_4 \rightarrow {}^7F_6$; 544 nm, $^5D_4 \rightarrow {}^7F_5$) and Eu^{3+} (579 nm, $^5D_0 \rightarrow {}^7F_0$; 651 nm, $^5D_0 \rightarrow {}^7F_3$; 700 nm $^5D_0 \rightarrow {}^7F_4$) can be obviously observed. The peaks at 592 and 617 nm may be the overlap of Eu^{3+} (591, 613 nm for $^5D_0 \rightarrow {}^7F_{1,2}$) and Tb^{3+} (589, 622 nm for $^5D_4 \rightarrow {}^7F_{3,4}$). Similarly, the integration of three emission bands (blue for modified host, red for Eu^{3+} and green for Tb^{3+}) can be realized to white color emission output. While for the luminescent spectrum of S-phen-Eu-ABA-[ZA-Tb-bipy] hybrids in Figure 7 (b) with the same measure condition, both excitation and emission spectra show the similar band position to Figure 7 (a) except for the distinct intensity of the spectrum for organically modified host. For its emission spectrum, only a weak broad emission broad is checked in the visible region centered at 448 nm for modified host, while a strong characteristic emission of Ln^{3+} with sharp bands at 489, 545, 579, 590, 618, 651 and 699 nm appear. Among the former two bands is corresponded to f-f transitions of Tb^{3+} ($^5D_4 \rightarrow {}^7F_J$, J = 6, 5) and the bands at 579, 651 and 699 nm are for Eu^{3+} ($^5D_0$ - ^7F_J, J = 0, 3, 4). The emission bands at 590, 618 nm are mainly due to the emission of Eu^{3+}, which may integrates the emission of Tb^{3+} (589, 622 nm for $^5D_4 \rightarrow {}^7F_{4,3}$). Based on the difference of the two spectra, it can be predicted that the energy transfer to lanthanide ions in S-phen-Eu-ABA-[ZA-Tb-bipy] hybrids is more effectively than that in S-phen-Eu-HBA-[ZA-Tb-bipy] one. The excitation and emission spectra of the S-phen-Eu-ABA-[ZA-Tb-TAA] (a) and S-phen-Eu-ABA-[ZL-Tb-bipy] (b) is shown in Figure S5. The excitation spectra is obtained by detecting the emission of Eu^{3+} at 613 nm and Tb^{3+} at 545 nm, respectively, both of which present the similar feature as that in Figure 7. The emission spectra of the two hybrids are also identical, showing the emission of functionalized host, Eu^{3+} and Tb^{3+}. Subsequently, the three kind of luminescence can display white luminescence.

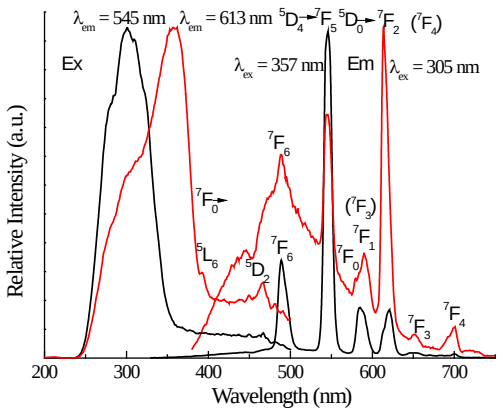

Figure 8 Luminescent spectra of hybrid materials S-phen-Tb-HBA-[ZA-Eu-TTA] hybrids

Figure 8 exhibits the excitation and emission spectra of S-phen-Tb-HBA-[ZA-Eu-TTA] hybrids. Different from the other hybrids, its excitation spectra are show different excitation peaks by monitoring the $^5D_4 \rightarrow {}^7F_5$ transition line of Tb^{3+} at 545 nm and $^5D_0 \rightarrow {}^7F_2$ transition line of Eu^{3+} at 613 nm, which are located at 305 nm and 357 nm, respectively. Correspondingly, the emission spectra are also different under the excitation of the two wavelengths. For excitation with 305 nm, the emission of Tb^{3+} is dominant, showing four sharp emission lines at 489, 546, 585 and 622 nm corresponding to the $^5D_4 \rightarrow {}^7F_6$, $^5D_4 \rightarrow {}^7F_5$, $^5D_4 \rightarrow {}^7F_4$ and $^5D_4 \rightarrow {}^7F_3$ transitions, respectively. While the emission of Eu^{3+} is weak and only the relative eminent emission band at 615 nm can be checked. On the contrary to the excitation with 357 nm, the emission intensity of Eu^{3+} is stronger

than that of Tb^{3+}. Therefore, the selective excitation of such hybrid system can tune the luminescence of different Ln^{3+}.

Table 1 The luminescent data of hybrid materials

Hybrid materials	λ_{ex}(nm)	λ_{em}(nm)	τ (μs)	η (%)
S-phen-Eu-HBA-[ZA-Tb-bipy]	298	613	504	25.8
S-phen-Tb-ABA-[ZL-Zn-bipy]	312	545	1087	93.3
S-phen-Tb-HBA-[ZA-Eu-TTA]	305	545	719	29.1
	357	613	524	94.0
S-phen-Eu-ABA-[ZL-Tb-bipy]	297	613	522	16.9
S-phen-Eu-ABA-[ZA-Tb-bipy]	341	613	221	90.2
S-phen-Eu-HBA-[ZA-Zn-bipy]	329	613	360	90.4
S-phen-Eu-ABA-[ZA-Tb-TAA]	319	613	360	12.1

τ, lifetime for $^5D_4 \rightarrow {}^7F_5$ transition of Tb^{3+} and $^5D_0 \rightarrow {}^7F_2$ transition of Eu^{3+}; η, the emission quantum efficiency.

To further investigate the luminescence performance of these multi-component hybrid materials, the typical decay curves of them are measured and the luminescent lifetimes for dominant emissive Eu^{3+} ($^5D_0 \rightarrow {}^7F_2$) or Tb^{3+} ($^5D_4 \rightarrow {}^7F_5$). The resulting lifetime data of these hybrid materials are summarized in Table 1. It can be seen that the luminescent lifetimes of the Tb^{3+} ($^5D_4 \rightarrow {}^7F_5$) emission are longer than those of the Eu^{3+} ($^5D_0 \rightarrow {}^7F_2$) one. This may be due to the fact that the energy match between HBA or ABA and Tb^{3+} is more effective than Eu^{3+}.[30] Moreover, the absolute luminescence quantum yield data can be obtained on condition that they are accurately performed with an integrating sphere and a calibrated detector setup for solid materials (the data also shown in Table 1). The luminescent quantum efficiency data do not show the apparent rule. This perhaps is due to the luminescent species and building units are complicated in the multi-component hybrid systems. Among, four kinds of hybrid systems, S-phen-Tb-ABA-[ZL-Zn-bipy], S-phen-Tb-HBA-[ZA-Eu-TTA], S-phen-Eu-ABA-[ZA-Tb-bipy] and S-phen-Eu-HBA-[ZA-Zn-bipy] possess the high quantum efficiencies of 90 %, which are higher than those of both lanthanide complexes modified microporous Zeolite (A/L) hybrids[21] and lanthanide complexes modified mesoporous SBA-15 hybrids[14,15]. So the multicomponent hybrid systems can achieve the benefit luminescent quantum efficiencies for the integration of different functional units, which is favorable for the further practical application.

Furthermore, the CIE chromaticity diagrams of these hybrid materials are checked, which are shown in Figure 9 and Figure S6, respectively. For the emission spectra in Figures 6(a), 7(a) and S5, the emission of organically modified host, Eu^{3+} and Tb^{3+} all appear and so the white color luminescence can be integrated with suitable excitation wavelength. Subsequently, it can be found the four hybrid systems (S-phen-Eu-HBA-[ZA-Zn-bipy], S-phen-Eu-HBA-[ZA-Tb-bipy], S-phen-Eu-ABA-[ZA-Tb-TAA] and S-phen-Eu-ABA-[ZL-Tb-bipy]) emit close white luminescence (Figure 9(a)-(d)), whose CIE coordinates ((0.2947, 0.2982), (0.2878, 0.2807), (0.3587, 0.3360) and (0.2984, 0.3502)), respectively, are in the white region, which is useful for the lighting. For S-phen-Tb-ABA-[ZA-Zn-bipy] hybrids in Figure S6 (a), the dominant emission of Tb^{3+} produces the luminescent color in green region (0.3096, 0.5930). For S-phen-Eu-ABA-[ZA-Tb-bipy] hybrids in Figure S6 (b), the emission integration of both Eu^{3+} and Tb^{3+} appears the close cool-white region (0.3457, 0.3675). For S-phen-Tb-HBA-[ZA-Eu-TTA] hybrids, different excitation wavelengths produce different emissive colors: Figure S6(c) is similar green region (0.3219, 0.5480) under excitation of 305 nm for dominant emissive Tb^{3+}. While under excitation of 357 nm for dominant emissive Eu^{3+} (Figure S6 (d)), the luminescent color shifts to near white region (0.2984, 0.3502). Combined with the white luminescence and higher quantum yields, the two kinds of multi-component hybrids S-phen-Tb-ABA-[ZL-Zn-bipy] and S-phen-Eu-ABA-[ZA-Tb-bipy] will be expected to have potential application value.

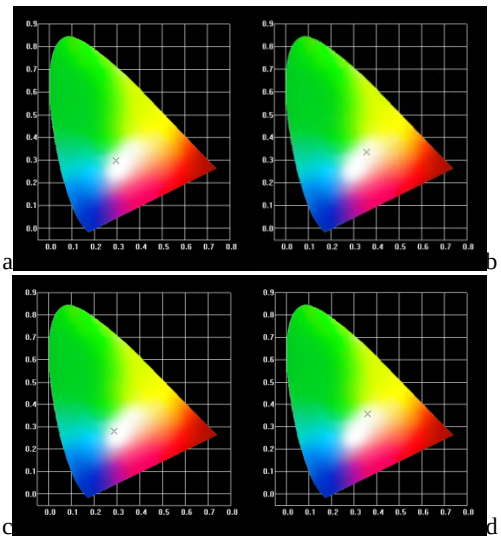

Figure 9 The CIE diagrams of hybrid materials for white color luminescence: (a) S-phen-Eu-HBA-[ZA-Zn-bipy], (b) S-phen-Eu-HBA-[ZA-Tb-bipy], (c) S-phen-Eu-ABA-[ZA-Tb-TAA] and (d) S-phen-Eu-ABA-[ZL-Tb-bipy])

Conclusion

In summary, several kinds of novel micro-mesoporous multi-component hybrid materials have been prepared by assembling both functionalized zeolite A/L and modified SBA-15 host through the two organically grafted silane linkers and coordination reaction of lanthanide ions. The mesoporous ordering microstructure is remained and the microporous crystal state is affected. By adjusting the different emissive center in the hybrid system, the multi-color luminescence can be obtained and even the white color luminescence can be integrated for four kinds of hybrids. Meanwhile, the combination of different emissive species in the hybrids achieves the high luminescent quantum efficiencies. These research results provide the strategy to assemble novel kind of multi-component hybrid materials, which is useful to have potential applications in optical device for display and lighting.

Acknowledgements

This work was supported by the National Natural Science Foundation of China (91122003) and Developing Science Funds of Tongji University.

Notes and references

[a] Department of Chemistry, Tongji University, Shanghai, 200092, China.
E-mail: byan@tongji.edu.cn; Fax: +86-21-65982287;
Tel: +86-21-65984663

† Electronic Supplementary Information (ESI) available: [details of any supplementary information available should be included here]. See DOI: 10.1039/b000000x/

1 (*a*) J. C. G. Bunzli and C. Piguet, *Chem. Rev.*, 2002, **102**, 1897; (*b*) D. Parker, *Chem. Soc. Rev.*, 2004, **33**, 156; (*c*) S. V. Eliseeva and J. C. G. Bunzli, *Chem. Soc. Rev.*, 2010, **39**, 189.

2 (*a*) C. P. Montgomery, B. S. Murray, E. J. New, R. Pal and D. Parker, *Acc. Chem. Res.*, 2009, **42**, 925; (*b*) K. L. Haas and J. Katherine, *Chem. Rev.*, 2009, **109**, 4921; (*c*) J. C. G. Bunzli, *Chem. Rev.*, 2010, **110**, 2729.

3 (*a*) L. D. Carlos, R. A. S. Ferreira, V. D. Bermudez and S. J. L. Ribeiro, *Adv. Mater.*, 2009, **21**, 509; (*b*) K. Binnemans, *Chem. Rev.*, 2009, **109**, 4283.

4 (*a*) B. Yan, *RSC Adv.*, 2012, **2**, 9304; (*b*) J. Feng, H. J. Zhang, *Chem. Soc. Rev.*, 2013, **42**, 387.

5 (*a*) D. F. Parra, H. F. Brito, J. D. R. Matos and L. D. Carlos, *J. Appl. Polym. Sci.*, 2002, **83**, 2716; (*b*) M. C. Goncalves, N. J. O. Silva, V. D. Bermudez, R. A. S. Ferreira, L. D. Carlos, K. Dahmouche, C. V. Santilli, D. Ostrovskii, I. C. C. Vilela and A. F. Craievich, *J. Phys. Chem. B*, 2005, **109**, 20093.

6 (*a*) G. De Cremer, B. F. Sels, J. I. Hotta, M. B. Roeffaers, E. Bartholomeeusen, E. Coutiño−Gonzalez, V. Valtchev, D. E. De Vos, T. Vosch and J. Hofkens, *Adv. Mater.*, 2010, **22**, 957; (*b*) P. Lenaerts, A. Storms, J. Mullens, J. D'Haen, C. Görller-Walrand, K. Binnemans and K. Driesen, *Chem. Mater.*, 2005, **17**, 5194; (*c*) B. H. Kwon, H. S. Jang, H. S. Yoo, S. W. Kim, D. S. Kang, S. Maeng, D. S. Jang, H. Kimand D. Y. Jeon, *J. Mater. Chem.*, 2011, **21**, 12812.

7 (*a*) H. R. Li, J. Lin, H. J. Zhang, H. C. Li, L. S. Fu and Q. G. Meng, *Chem. Commun.*, 2001, 1212; (*b*) Q. M. Wang, and B. Yan, *J. Mater. Chem.*, 2004, **14**, 2450.

8 (*a*) L. Guo and B. Yan, *Eur. J. Inorg. Chem.*, 2010, 1267; (*b*) J. L. Liu and B. Yan, *Dalton Trans.*, 2011, **40**, 1961; (*c*) P. Liu, H. R. Li, Y. G. Wang, B. Y. Liu, W. J. Zhang, Y. J. Wang, W. D. Yan, H. J. Zhang and U. Schubert, *J. Mater. Chem.* 2008, **18**, 735; (*d*) Z. M. Hao, X. Z. Song, M. Zhu, X. Meng, S. N. Zhao, S. Q. Su, W. T. Yang, S. Y. Song and H. J. Zhang, *J. Mater. Chem. A*, 2013, **1**, 11043.

9 J. L. Liu and B. Yan, *J. Phys. Chem. B*, 2008, **112**, 10898.

10 B. Yan and H. F. Lu, *Inorg. Chem.*, 2008, **47**, 5601.

11 B. Yan and X. F. Qiao, *J. Phys. Chem. B*, 2007, **111**, 12362.

12 Y. F. Shao and B. Yan, *Dalton Trans.*, 2012, **41**, 7423.

13 (*a*) J. Feng, S. Y. Song, Y. Xing, H. J. Zhang, Z. F. Li, L. N. Sun, X. M. Guo and W. Q. Fan, *J. Solid State Chem.* 2009, **182**, 435; (*b*) J. Feng, S. Y. Song, W. Q. Fan, L. N. Sun, X. M. Guo, C. Y. Peng, J. B. Y. N. Yu and H. J. Zhang, *Microp. Mesop. Mater.*, 2009, **117**, 278; (*c*) B. Yan, B. Zhou and Y. Li, *Microp. Mesop. Mater.*, 2009, **120**, 317; (*d*) Q. G. Meng, P. Boutinaud, A. C. Franville, H. J. Zhang and R. Mahiou, *Microp. Mesop. Mater.*, 2003, **65**, 127.

14 (*a*) L. N. Sun, S. Dang, J. B. Yu, J. Feng, L. Y. Shi and H. J. Zhang *J. Phys. Chem. B*, 2010, **114**, 16393; (*b*) Y. Li, B. Yan and Hong Yang, *J. Phys. Chem. C*, 2008, **112**, 3959

15 (*a*) Y. J. Li, B. Yan, *Dalton Trans.* 2010, **39**, 2554; (*b*) X. M. Guo, H. D. Guo, L. S. Fu, R. P. Deng, W. Chen, J. Feng, S. Dang and H. J. Zhang, *J. Phys. Chem. C*, 2009, **113**, 2603.

16 N. Gfeller, S. Megelski and G. Calzaferri, *J. Phys. Chem. B*, 1998, **102**, 2433.

17 (*a*) A. Mech, A. Monguzzi, F. Meinardi, J. Mezyk, G. Macchi and R. Tubino, *J. Am. Chem. Soc.*, 2010, **132**, 4574; (*b*) A. Zabala Ruiz, H. Li and G. Calzaferri, *Angew. Chem.*, 2006, **118**, 5408(*c*)

18 (*a*) P. Li, Y. Wang, H. Li and G. Calzaferri, *Angew. Chem. Int. Edi.*, 2014, **53**, 2904; (*b*) G. Calzaferri, S. Huber, A. Devaux, A. Z. Ruiz, H. Li, O. Bossart and L. Q. Dieu, *Proc. of SPIE, Org. Optoelectronics and Photonics II*, 2006, **619**, 216.

19 (*a*) Y. Feng, H. R. Li, Q. Y. Gan, Y. G. Wang, B. Y. Liu and H. J. Zhang, *J. Mater. Chem.*, 2010, **20**, 972; (*b*) H. S. He, M. Dubey, A. G. Sykes and P. S. May, Stanley, *Dalton Trans.*, 2010, **39**, 6466.

20 (*a*) S. Y. Choi, Y. J. Lee, Y. S. Park, K. Ha and K. B. Yoon, *J. Am. Chem. Soc*, 2000, **122**, 5201; (*b*) S. Gago, J. A. Fernandes, J. P. Rainho, R. A. Sá Ferreira, M. Pillinger, A. A. Valente, T. M. Santos, L. D. Carlos, P. J. Ribeiro-Claro and I. S. Gonçalves, *Chem. Mater.*, 2005, **17**, 5077.

21 (*a*) Z. Popović, M. Busby, S. Huber, G. Calzaferri and L. De Cola, *Angew. Chem. Int. Ed.*, 2007, **46**, 8898; (*b*) J. N. Hao and B. Yan, *Dalton Trans.*, 2014, **43**, 2810.

22 D. Zhao, J. Feng, Q. Huo, N. Melosh, G. H. Fredrickson, B. F. Chmelka and G. D. Stucky, *Science*, 1998, **279**, 548.

23 D. Zhao, Q. Huo, J. Feng, B. F. Chmelka and G. D. Stucky, *J. Am. Chem. Soc.*, 1998, **120**, 6024.

24 A. Z. Ruiz, D. Bruhwiler, T. Ban and G. Calzaferri, *Monatsh. Chem.*, 2005, **136**, 7.

25 Q. M. Wang and B. Yan, *J. Organomet. Chem.*, 2006, **691**, 540.

26 J. F. Wang, H. Li, J. J. Zhang, N. Ren and K. Z. Wu, *Sci. China Chem.*, 2012, **55**, 2161.

27 C. Y. Peng, H. J. Zhang, J. B. Yu, Q. G. Meng, L. S. Fu, H. R. Li, L. N. Sun and X. M. Guo, *J. Phys. Chem. B*, 2005, **109**, 15278.

28 X. Wang, K. S. K. Lin, J. C. C. Chan and S. Cheng, *J. Phys. Chem. B*, 2005, **109**, 1763.

29 J. G. DeShazer and G. H. Dieke, *J. Chem. Phys.*, 1963, **38**, 2190.

30 B. Yan, H. J. Zhang, S. B. Wang and J. Z. Ni, *Monatsh. Chem.*, 1998, **129**, 151.

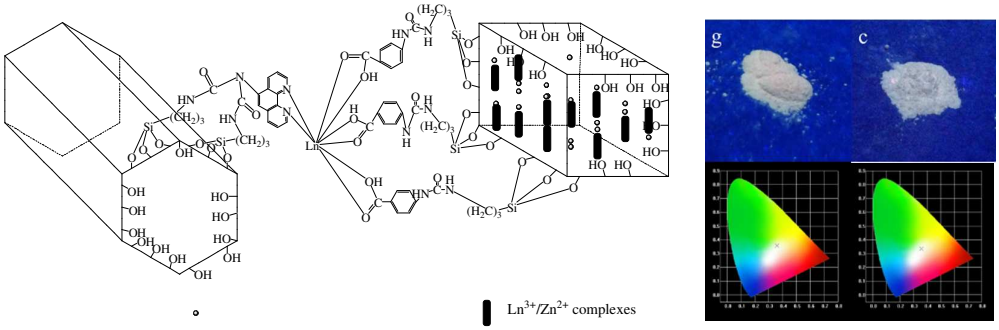

In summary, several kinds of novel micro-mesoporous multi-component hybrid materials have been prepared by assembling both functionalized zeolite A/L and modified SBA-15 host through the two organically grafted silane linkers and coordination reaction of lanthanide ions. The white color luminescence can be integrated by adjust the different emissive center and high quantum efficiencies can be obtained.